# RECONFIGURABLE DIGITAL METASURFACE FOR 3-BIT PHASE ENCODING

*Shengya Zhao* *Robert Langwieser* *Christoph F. Mecklenbräuker*

Institute of Telecommunications, TU Wien, Vienna, Austria
shengya.zhao@tuwien.ac.at

## ABSTRACT

In this contribution, we propose, design, simulate and prototypically realize a 3-bit digital coding metasurface by controlling the phase and amplitude response of the metasurface, which is applicable to a wireless telecommunication system as a transmitter. The proposed metasurface consists of metal patches on a dielectric substrate and varactors, which allow controlling the phase and amplitude of the metasurface's reflected wave by the varactors' bias voltages.

***Index Terms***— digital metasurface; 6G; anomalous reflection, beamforming and precoding, massive MIMO

## 1. INTRODUCTION

Metasurfaces have shown the capability to control the reflection, transmission, and polarization of electromagnetic waves and recently have attracted much attention by researchers in telecommunications [1, 2, 3, 4, 5, 6]. The generalized Snell's law proposed by Yu et al. [7], laid a theoretical foundation for metasurfaces by showing that anomalous reflection and refraction of electromagnetic waves are achievable when a suitable phase gradient is realizable at the metasurface [7]. In the meantime, inspired by generalized Snell's law, many different materials, surface structures, and technologies have been proposed for realizing metasurfaces [8]. In the last decade, from the initial analog metasurface, where the metasurface was approximated by equivalent capacitance and inductance [9], towards the digital metasurface [10], metasurfaces have experienced rapid development.

Through the control over the metasurface element's geometries and orientations or electrical characteristics, it is possible to create varying phase and amplitude discontinuities along the patterned interface. It has been verified that a 2-bit digital signal modulator for quadrature phase-shift keying (QPSK) is realizable as a metasurface [11]. Recently, a 1-bit Reconfigurable Intelligent Surface (RIS) with 1100 controllable elements working in the 5.8 GHz band was proposed to prototype a RIS-aided wireless communication system. A real-time over 500 m long-range outdoor RIS assisted wireless communication system was achieved to realize a video signal transmission, providing a 14 dB gain compapre with the szstem without RIS, and delivering 32 Mbps using only 23 dBm of transmit power [12].

Commercial state-of-the-art devices for wireless communication require several building blocks in hardware to realize digital signal modulation and transmission, e.g. analog filters, amplifiers, digital-to-analog converters, voltage controlled oscillators. In contrast, the digital coding metasurface is capable of modulating a carrier wave with the information bearing signal directly, which may prove to be a reduction in hardware complexity.

In this contribution an encoding metasurface is designed, simulated and manufactured which consists of metal patches on a dielectric substrate and varactors. The reverse bias voltage of the varactors allows to control the phase of the metasurface's reflected wave. Finally, the prototypically realized 3-bit digital encoding metasurface is characterized by measurements of the phase and absolute amplitude response.

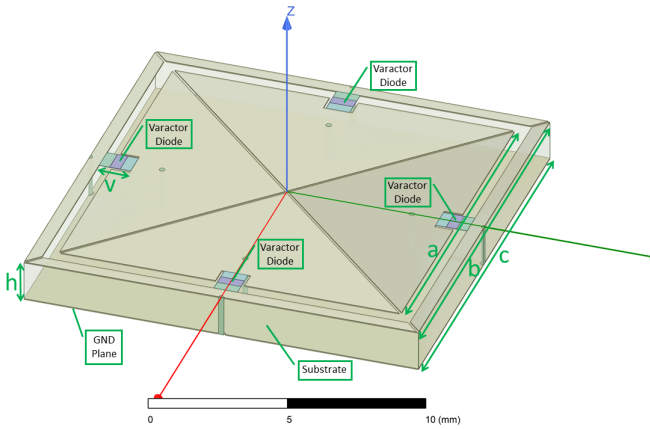


**Fig. 1**: Model of metasurface unit element, which consists of metal patches on a dielectric substrate and 4 varactors.

## 2. DESIGN OF UNIT ELEMENT

The proposed unit element of the metasurface is shown in Fig. 1 based on ideas in [13, 14]. The unit element is a cuboid volume with dimensions $15\,\mathrm{mm} \times 15\,\mathrm{mm} \times 1.524\,\mathrm{mm}$. The detailed geometrical parameters in Fig. 1 are as follows: $a = 13\,\mathrm{mm}$, $b = 14\,\mathrm{mm}$, $c = 15\,\mathrm{mm}$, thickness of substrate $h =$

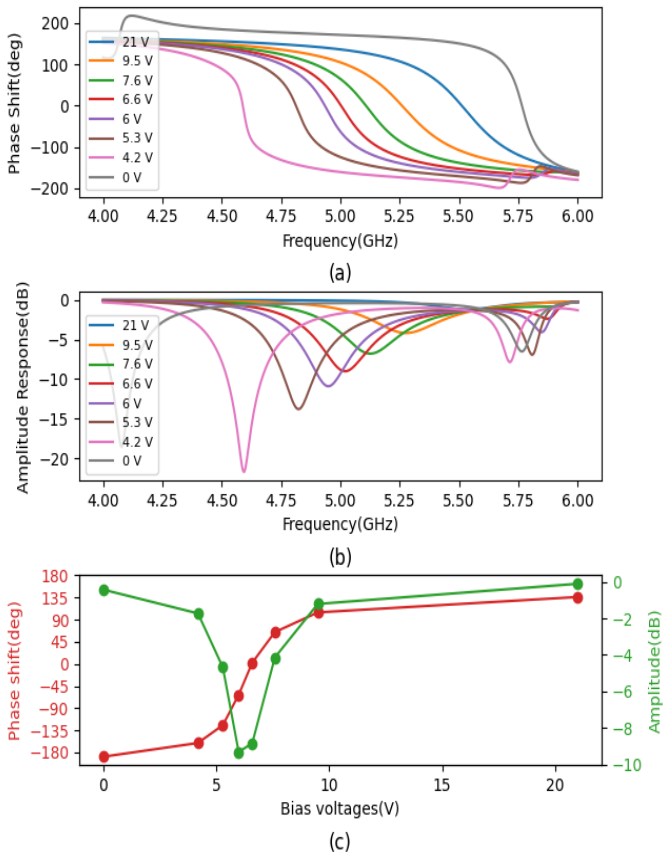


**Fig. 2**: Numerical simulation: (a) Metasurface phase response under 8 different varactors' bias voltages over frequency range 4–6 GHz, (b) Metasurface amplitude response in dB under 8 different varactors' bias voltages over frequency range 4–6 GHz, (c) Phase shift and amplitude response at 5 GHz

$1.524\,\text{mm}$, and the varactor size $v = 1.5\,\text{mm}$. The top surface consists of copper frame and a central copper patch, the bottom surface is also covered by copper, the thickness of all copper layers are $t_m = 0.0347\,\text{mm}$. Between the top and ground copper layers is Rogers RO4003 substrate located, with relative permittivity $\varepsilon_r = 3.55$ and dielectric loss tangent $\tan(\delta) = 0.0027$.

## 3. SIMULATION FOR INFINITE METASURFACE

For the purpose of numerical simulation we assume that the metasurface is a planar periodic arrangement of unit elements and infinitely large in aperture. Bloch's theorem states that solutions to the Helmholtz equation with periodic boundary conditions take the form of a plane wave modulated by a periodic function [15]. We take advantage of the periodic boundary conditions by numerically simulating only a single unit element.

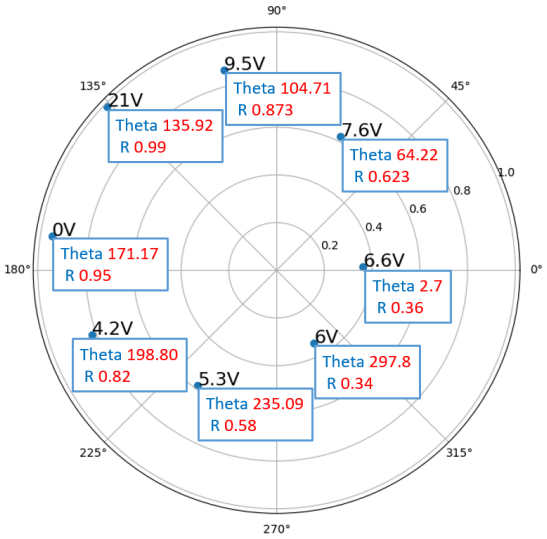


**Fig. 3**: Numerical simulation of phase/normalized amplitude response of the metasurface for different varactor bias voltages resulting in an approximate 8-PSK constellation at 5GHz.

A homogeneous plane wave with linear polarization state is illuminating the metasurface at normal incidence, i.e. direction of arrival $0°$. For the purpose of comparison to mesaurements in experiments, we set up the simulation scenario to compute the phase shift of the reflected wave in direction $45°$.

The simulation results are shown in Fig. 2. The phase and amplitude response of the reflected wave are Figs. 2(a) and 2(b), respectively. At $5\,\text{GHz}$, the resulting phase shifts and amplitude responses at eight different varactor's bias voltages are shown as the marked points in Fig. 2(c). All the marked points in Fig. 2(c) are converted to the constellation diagram, which shown in figure 3. We can see that, at $5\,\text{GHz}$, the resulting phase shifts and normalized amplitude responses at eight different varactor's bias voltages for 8-PSK are achieved. The adjacent states present an approximate $\pi/4$ phase shift distance, and all eight states possess large enough amplitude.

With the above achieved simulation results, the metasurface can be applied as a digital signal modulator on the transmitter side in a wireless communication system, where a transmitted plane wave is emitted on the digital metasurface and reflected by it. Via changing the metasurface varactors' bias voltages, the reflected wave obtains a specific phase shift base on specific bias voltage. These different phase shifts have $\pi/4$ phase distance. At the same time, the amplitudes of the reflected waves do not change significantly, they all stay between $0dB$ to $-9dB$. When using a constellation diagram to show all the reflected phase shifts and amplitude changes, as shown in Fig. 3, we can clearly see clearly that the applied metasurface realizes a 8 states (3 bits) phase-shift-keying

(8-PSK). Furthermore, when changing the amplitude of the incident plane wave, it is even possible to realize 16-PSK or more. This describes the strategy of digital coding metasurface, that the digital signal can be represented by the bias voltage of metasurface, and be transmitted directly on the reflected wave by a metasurface. This performance determines if the metasurface can directly load the digital signal into the reflected electromagnetic wave and emit it.

## 4. EXPERIMENTAL SETUP AND RESULT

Next, the phase of the reflected wave from the metasurface is validated under eight different bias voltages and the measurement results are compared with the numerical simulation. Finally, for testing the transmission accuracy of metasurface assisted wireless transmission, we use 80 random reverse bias voltages and evaluate the message error rate of transmission.

### 4.1. Manufactured metasurface and experimental setup

For the experimental characterization, we manufactured a $6 \times 6$ array of unit elements as shown in Fig. 4. Each unit element includes four varactor diodes, so the 36-element metasurface contains 144 varactor diodes. Reverse bias voltages are applied to each metasurface unit's varactor diodes through the copper bottom layer and vias in the metasurface substrate. The size of the printed circuit board is $135\,\mathrm{mm} \times 125\,\mathrm{mm}$ and the array of unit elements which constitutes the metasurface has an aperture of $90\,\mathrm{mm} \times 90\,\mathrm{mm}$, which is the metal-covered area. The surrounding frame in red color is the solder mask which does not contribute to variable phase shifts of the reflected wave.

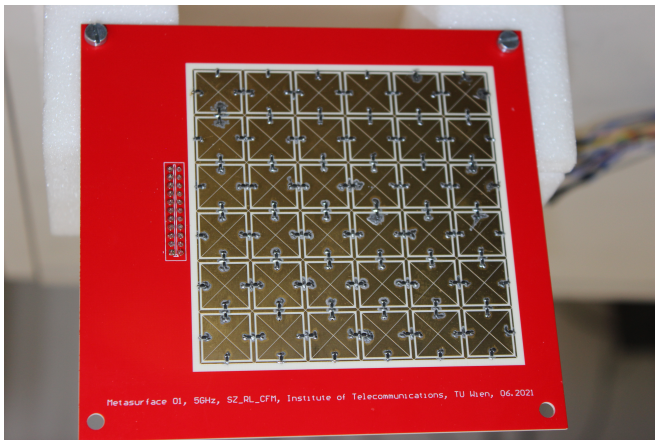


**Fig. 4**: Manufactured metasurface, which is a $6 \times 6$ array of metallic patches on a dielectric substrate and 144 varactors.

Figure 5 shows our experiment setup. The wave emitted by transmitter horn antenna Tx will reach the metasurface perpendicularly (with $90°$ incident angle), and horn antenna Rx is used as receiver antenna, which is in $45°$ degree direction to

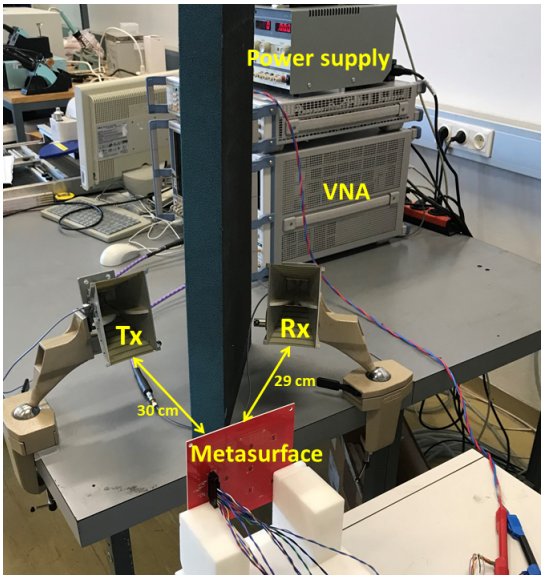


**Fig. 5**: Setup used for lab measurements with R&S ZVA8, two horizontally polarized ridged horn antennas and TTi PL330DP power supply for controlling varactor DC bias voltages.

metasurface, to detect and receive the reflected wave by metasurface. This position setup is the same as in the HFSS simulation. Horn antenna Tx and Rx are connected to the Vector Network Analyser (VNA) port one and two, respectively. The VNA measures the complex forward transmission coefficient $S_{21}$ characterizing the phase and absolute amplitude response of the reflected wave. The VNA provides 10dBm power to Tx. A power supply is connected with the metasurface to provide eight stable DC voltages (21V, 9.5V, 7.6V, 6.6V, 6V, 5.3V, 4.2V, 0V) to metasurface, which are bias voltages for the varactor diodes mounted on the metasurface. One voltage will be applied to all metasurface units at one time. The distance from Horn antenna Tx and Rx to the metasurface is 30cm and 29cm. As the Tx and Rx antennas are close to each other, we put an absorbing material, the blue-black block, between them to avoid the interference between them.

### 4.2. Phase shift response test

Throughout the experiment, the emitted wave from horn antenna Tx is constant, and the antenna Rx also continuously detects the incident wave's phase and amplitude response. As the bias voltage applied to the metasurface changes, the detected phase and amplitude response of the received reflected wave will also change accordingly.

By sequentially adding the eight different bias voltages to the metasurface, eight different phase and amplitude responses are obtained at the receiver side. In frequency range 4.9 GHz to 5.1 GHz, the experiment results are plotted as shown in Fig. 6 (a), and the simulation results are shown in

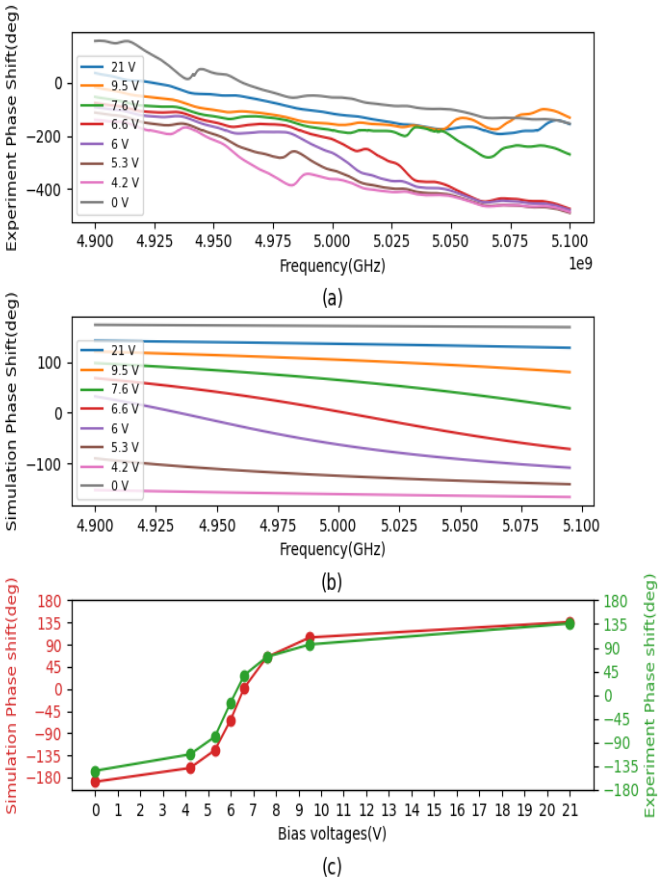


**Fig. 6**: Phase response of reflected horizontally polarized wave in 4.9 – 5.1 GHz band: (a) measurement, (b) simulation. (c) Experiment phase shift vs. simulation phase shift at 5 GHz

Fig. 6 (b). In order to better observe the regulation of the bias voltage on the reflected wave phase, we only extract the phase shift of simulation and experiment result at 5GHz, and get the relationship between bias voltages and reflected wave phase shift, and they are plotted in figure 6 (c). From the figures 6 (a) (b), we can see, in the experimental results, the phase shifts at lower bias voltages are a bit smaller than in simulation, The reason is that, in simulation, the incident waves of all frequencies have zero phases at the metasurface, but in the experiment, because of the distance from the incident antenna to metasurface, the incident waves at metasurface cannot achieve zero-phase for each frequency. The phase generated by the distance will be added to the reflected wave, resulting in a reduction in the phase shift of the reflected wave. But the overall trend is consistent with the simulation results as shown in figure 6 (c).

### 4.3. Stability of transmission with 3 bits metasurface

As the 3 bits metasurface uses the reverse bias voltages to add a phase shift to the incident wave, our metasurface is able to realize eight different phase shifts with eight reverse bias voltages, and there is approximately a $45^\circ$ interval between adjacent phase shifts. In other words, the metasurface can directly modulate the incident wave, add the voltage information to the transmitted wave. Eight reverse bias voltages represent eight different signals. Therefore, by detecting the phase shift of the reflected wave at the receiver side, the voltage applied on the metasurface can be determined, also the 3 bits information represented by the voltage. By comparing the demodulated voltages at the receiver side with the modulated voltages at the transmitter side, we can study and understand the stability of metasurface transmission.

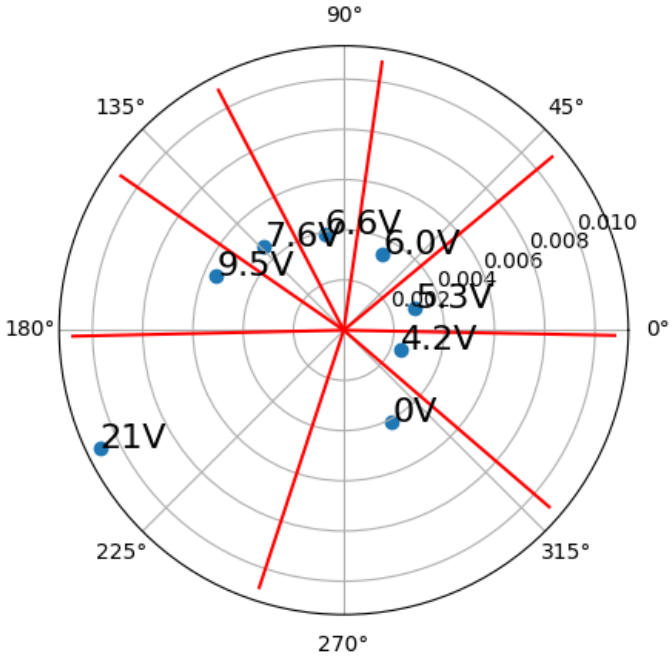


**Fig. 7**: Phase/absolute amplitude response of 8 pilot signal points at 5GHz expressed on polar coordinate system

In this experiment, first, we sequentially load eight different voltages on the metasurface as pilot signals, and then the receiver antenna transmits the reflected wave to VNA. VNA detects and analyses the phase shift of reflected signal at frequency 5GHz. The phase and absolute amplitude of eight signals at 5GHz are expressed on a polar coordinate system, as the signal points shown in figure 7. It can be seen that the eight different signal points distribute evenly on a 360-degree range. They are not exactly the same as the simulation phase results in figure 3, but the order of points and the interval between neighbor points are basically consistent with the simulation result.

With the eight points as pilot signals, the receiver gets the

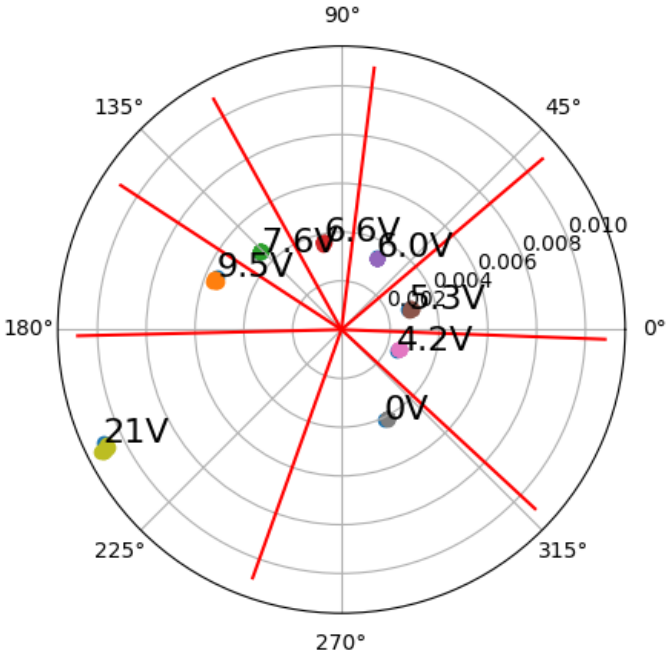


(a)

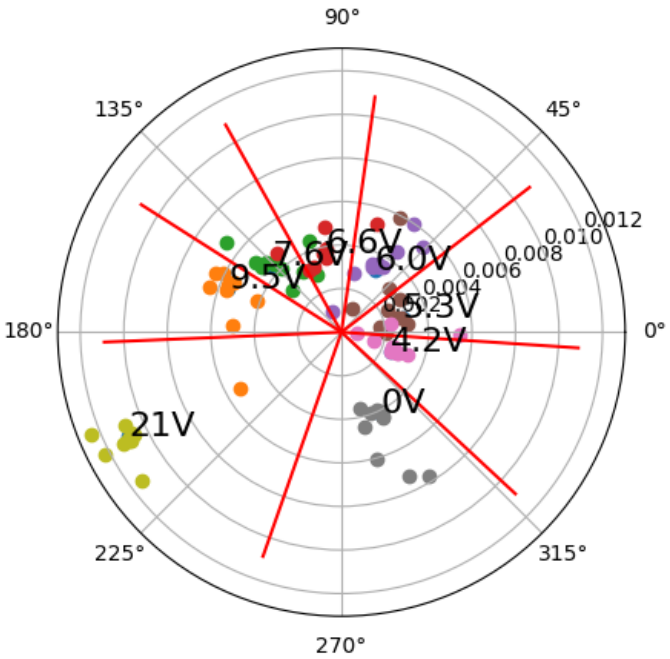


(b)

**Fig. 8**: At 5 GHz, the phase shift distribution of received signals, which are reflected by metasurface with 80 randomly generated reverse bias voltages (a) 80 demodulated test signal points in a static environment (b) 80 demodulated test signal points in dynamic environment.

relationship between the phase shift of the received signal and the bias voltages added on the metasurface. Therefore, the receiver can determine the metasurface reverse bias voltages based on the phase shift of the received reflected wave. The red line in figure 7 shows the decision boundaries. If the received signal falls into one of the pilot voltage Sector ranges, the received signal will be automatically demodulated as this pilot signal.

Next step, 80 bias voltages are generated randomly following a discrete uniform distribution, ten times for each one. When the surrounding environment is static, the detected phase shifts and decided reverse bias voltages all fall at the same position as the pilot signals. The result is shown in figure 8a. Now for the same experiment, but if the environment becomes dynamic, e.g., movement of persons close to the metasurface, the phase shift of received 80 signals are shown as in figure 8b.

By comparing the demodulated reverse bias voltages with the reverse bias voltages which are applied to the varactors of the metasurface, we observe that all 80 reverse bias voltages are correctly demodulated under a stable environment, the message error rate is 0. In a dynamic environment, 68 bias voltages are correctly demodulated, and the message error rate is 0.15.

Summarizing the above two experiments, from the phase shift response test, we can see an $8 \times 8$ metasurface with a size of only $90\,\mathrm{mm} \times 90\,\mathrm{mm}$, can already achieve phase-shift responses that are very close to the simulation result. It can be seen that the metasurface is very effective in regulating electromagnetic waves. And with the stability test, in a volatile test environment, our metasurface can still achieve a pretty stable signal transmission with a low message error rate, indicating that metasurface is a promising technology for electromagnetic wave control and wireless communication.

## 5. CONCLUSION

In summary, this study proposed, designed, manufactured, and measured a reconfigurable solid-state reflectarray comprising $6 \times 6$ elements which is controllable through the reverse biasing of varactors. This is usable as a 3-bit reconfigurable digital metasurface that realizes 8-PSK signal modulation at 5 GHz. The unit cell of the metasurface includes four varactor diodes. The metasurface is capable of any phase rotation of the reflected electromagnetic wave from $0^\circ$ to $360^\circ$. A metasurface with small aperture is shown to realize a relatively high regulation efficiency. At the same time, it can transmit eight different voltage signals steadily, which represent 3 bits digital signal. When excited by the carrier wave at 5 GHz, by adding eight different bias voltages on the metasurface, the reflected waves of the metasurface are modulated by a corresponding phase shift. We have measured the absolute amplitude and phase of the reflected electromagnetic wave and experimentally demodulated the carried informa-

tion based on the codebook into a corresponding reverse bias voltage signal (3-bit digital information stream) to recover the original information.

## 6. REFERENCES


[1] E. Basar, M. Di Renzo, J. De Rosny, M. Debbah, M.-S. Alouini, and R. Zhang. Wireless communications through reconfigurable intelligent surfaces. *IEEE Access*, 7:116753–116773, 2019.

[2] L. Dai, B. Wang, Min Wang, X. Yang, J. Tan, S. Bi, S. Xu, F. Yang, Z. Chen, M. Di Renzo, C.-B. Chae, and L. Hanzo. Reconfigurable intelligent surface-based wireless communications: Antenna design, prototyping, and experimental results. *IEEE Access*, 8:45913–45923, 2020.

[3] E. Björnson, Ö. Özdogan, and E. G. Larsson. Reconfigurable intelligent surfaces: Three myths and two critical questions. *IEEE Communications Magazine*, 58(12):90–96, 2020.

[4] Y.-C. Liang, J. Chen, R. Long, Z.-Q. He, X. Lin, C. Huang, S. Liu, X. S. Shen, and M. Di Renzo. Reconfigurable intelligent surfaces for smart wireless environments: channel estimation, system design and applications in 6g networks. *Science China Information Sciences*, 64(200301), 2021.

[5] A. Zappone and M. Di Renzo. Optimization of reconfigurable intelligent surfaces with electromagnetic field exposure constraints. In *Asilomar Conference on Signals, Systems, and Computing*, Pacific Grove (CA), USA, November 2021.

[6] L. Hao, S. Schwarz, and M. Rupp. Analysis and optimization of reconfigurable intelligent surfaces assisted MIMO systems. In *2021 Joint European Conference on Networks and Communications 6G Summit (EuCNC/6G Summit)*, pages 13–18, 2021.

[7] N. Yu et al. Light propagation with phase discontinuities: Generalized laws of reflection and refraction. *Science*, 334(6054):333–337, 2011.

[8] A. Nemati, Q. Wang, M. H. Hong, and J. H. Teng. Tunable and reconfigurable metasurfaces and metadevices. *Opto-Electronic Advances*, 1(5):1–25, 2018.

[9] D. Sievenpiper, L. Zhang, R. F. J. Broas, E. Yablonovitch, and N. G. Alexopolous. Corrections to "high-impedance electromagnetic surfaces with a forbidden frequency band". *IEEE Transactions on Microwave Theory and Techniques*, 48(4):620, 2000.

[10] T. J. Cui, M. Q. Qi, X. Wan, J. Zhao, and Q. Cheng. Coding metamaterials, digital metamaterials and programmable metamaterials. *Light: Science & Applications*, 3(10):e218, 2014.

[11] J. Y. Dai et al. Wireless communications through a simplified architecture based on time-domain digital coding metasurface. *Advanced Materials Technologies*, 4(7):1–8, 2019.

[12] X. Pei, H. Yin, L. Tan, L. Cao, Z. Li, K. Wang, K. Zhang, and E. Björnson. RIS-aided wireless communications: Prototyping, adaptive beamforming, and indoor/outdoor field trials. *Arxiv.org*, pages 1–13, Feb. 28 2021.

[13] G. Lasser, Z. Popović, and C. F. Mecklenbräuker. Dual-band, low-frequency artificial magnetic conductor using lumped components. In *2015 9th International Congress on Advanced Electromagnetic Materials in Microwaves and Optics (METAMATERIALS)*, pages 175–177, 2015.

[14] G. Lasser, L. W. Mayer, Z. Popović, and C. F. Mecklenbräuker. Low-profile switched-beam antenna backed by an artificial magnetic conductor for efficient close-to-metal operation. *IEEE Trans. Antenn. Propag.*, 64(4):1307–1316, April 2016.

[15] F. Bloch. Über die Quantenmechanik der Elektronen in Kristallgittern. *Zeitschrift für Physik*, A(52):555–600, 1929.